Sustainable Cities and Society 81 (2022) 103868

Contents lists available at ScienceDirect

Sustainable Cities and Society

journal homepage: www.elsevier.com/locate/scs

Solar energy harvesting pavements on the road: comparative study and performance assessment

Tao Ma [a,b,*], Senji Li [a,b], Wenbo Gu [c], Shengjie Weng [a,b], Jinqing Peng [d], Gang Xiao [e,*]

[a] School of Mechanical Engineering, Shanghai Jiao Tong University, Shanghai, China
[b] Engineering Research Ce ntre of Solar Energy and Refrigeration, Ministry of Education, China
[c] School of Electrical Engineering, Xinjiang University, Urumqi, Xinjiang, China
[d] College of Civil Engineering, Hunan University, Changsha, China
[e] State Key Laboratory of Clean Energy Utilization, Zhejiang University, Hangzhou, China

ARTICLE INFO

Keywords:
Solar energy harvesting pavements
Distributed energy generators
Performance comparison
Urban microclimate
Urban heat island (UHI)

ABSTRACT

As a significant infrastructure in modern cities, road pavements occupy a great share of urban surfaces and absorb abundant solar radiation. Thus, pavements have tremendous potential in solar energy utilization and can serve as distributed energy generators in smart and sustainable cities. Some solar energy harvesting pavement modules have emerged in recent years, including pavement-integrated photovoltaic (PIPV) module, pavement-integrated solar thermal (PIST) module, and pavement-integrated photovoltaic thermal (PIPVT) module. In this study, for all the above modules, simulations were conducted with the developed and validated two-dimensional transient models on the weather conditions of four typical days in different seasons in Shanghai. Both the operating performance and influence on the urban heat island (UHI) effect were investigated to evaluate and compare their energy performance and effect on urban microclimatic conditions. The results show that the electricity yield of the PIPVT module is slightly higher than that of the PIPV module, while its heat yield is lower than that of the PIST module on all typical days. When considering both electricity and heat yields, the PIPVT module can achieve an average overall energy efficiency of 37.31%. Compared with the conventional pavement module, all three solar energy harvesting pavement modules have lower maximum asphalt average temperatures that can decelerate the thermal aging of asphalt concrete. The PIPVT module has the most significant effect on the reduction of the maximum asphalt average temperature, decreasing it by 10.57°C on average. Additionally, all three solar energy harvesting pavement modules can mitigate the UHI effect, and the PIPVT and PIST modules have the most and the least influence on UHI effect mitigation, respectively.

1. Introduction

To promote environmentally sustainable cities and society, renewable energies are now widely used as alternatives to traditional fossil fuels that have caused severe air pollution and global warming (Javed et al., 2021; Ma et al., 2015). As an essential renewable energy resource, solar energy has been utilized in various applications (Ma et al., 2014). In conventional application scenarios, solar energy harvesting systems are installed in open ground areas, building roofs, and facades (Javed et al., 2019). However, in modern cities, the available land is very limited for the installation of solar energy systems, and systems on building roofs or facades will increase building load with a safety risk. Hence, in this context, urban pavements have emerged as a new scenario to harvest solar energy in recent years. Pavements can absorb a significant share of solar energy up to 40 MJ/m^2/day on hot summer days (Yang et al., 2021). As an essential infrastructure, pavements occupy 30–45% of the urban surfaces. Additionally, pavements' traffic density is relatively low when solar radiation is intensive around noon, indicating that few cars or pedestrians would shadow the road surface when the weather conditions are most suitable for solar energy harvesting of the day. Due to these advantages, pavements are regarded as promising substitutes that have enormous potential to harvest solar energy, especially in modern cities where the land is very limited. Thus, pavements have been utilized to harvest solar energy with the integration of several technologies and several pavement-integrated solar energy harvesting modules have been proposed in recent years, including pavement-integrated photovoltaic (PIPV) module, pavement-integrated solar thermal (PIST) module, and pavement-integrated photovoltaic thermal (PIPVT) module.

* Corresponding author.
E-mail addresses: tao.ma@sjtu.edu.cn (T. Ma), xiaogangtianmen@zju.edu.cn (G. Xiao).

https://doi.org/10.1016/j.scs.2022.103868
Received 13 November 2021; Received in revised form 25 February 2022; Accepted 27 March 2022
Available online 29 March 2022

Nomenclature

A_c	Collector area (m^2)
L	Length of the module (m)
W	Width of the module (m)
C	Specific heat capacity ($J \cdot kg^{-1} \cdot K^{-1}$)
E	Energy (J)
$\dot{E}$	Power (W)
$\ddot{E}$	Power per unit area ($W \cdot m^{-2}$)
h	Heat transfer coefficient ($W \cdot m^{-2} \cdot K^{-1}$)
k	Thermal conductivity ($W \cdot m^{-1} \cdot K^{-1}$)
$\dot{m}$	Mass flow rate ($kg \cdot s^{-1}$)
N	Number
T	Temperature (K)
D	Diameter (m)
V	Volume (L)
Re	Reynolds number
Nu	Nusselt number
Pr	Prandtl number
t	Time (s)
G	Horizontal solar radiation ($W \cdot m^{-2}$)
e	Efficient
v	Velocity ($m \cdot s^{-1}$)

Greek number

α	Absorptivity
η	Energy efficiency (%)
ς	Exergy efficiency (%)
ε	Emissivity
σ	Stefan-Boltzmann constant ($W \cdot m^{-2} \cdot K^{-4}$)
ρ	Density ($kg \cdot m^{-3}$)
δ	Thickness (m)
β	Photovoltaic temperature coefficient (%/°C)
τ	Transmissivity
γ	Reflectivity

Subscript

amb	Ambient environment
rfl	Reflection
sur	Pavement surface
sky	Sky
PV	Photovoltaic module
tub	Tubes
as	Asphalt concrete
ele	Electrical
th	Thermal
all	Overall
flu	Fluid
gla	Anti-slip front tempered glass
al	Aluminum baseplate
in	Inlet
out	Outlet
ref	Reference
t	Time
i	Inner
o	Outer
tank	Water tank
wind	Wind around the module
c	Conductive heat transfer
v	Convective heat transfer
r	Radiative heat transfer
$i-j$	Between i and j
sun	Incident solar radiation

Abbreviation

PV	Photovoltaic
PIPV	Pavement-integrated photovoltaic
PIST	Pavement-integrated solar thermal
PIPVT	Pavement-integrated photovoltaic thermal
UHI	Urban heat island
CP	Conventional pavement

The PIPV module, also known as photovoltaic (PV) pavement or PV floor tile, combines the conventional asphalt pavement and the PV panel. Hence, it can generate electricity besides the conventional function of withstanding the pedestrian and vehicle load. Ma et al. (2019) developed and fabricated two PIPV module prototypes with different anti-slip surfaces. The results of both laboratory and outdoor tests showed the prototypes could achieve satisfactory mechanical, thermal and electrical performance, implying that such PIPV modules could be a suitable replacement for the conventional pavements. Liu et al. (2019) proposed a novel framework to predict and calculate the harvested solar energy and the generated electricity on the roads, confirming that PV pavements have great potential to charge moving cars as an excellent supplement of city power. Zhou et al. (2020) adopted two types of PIPV modules with different structures and studied the effects of structure length, structure width, bottom plate thickness, grid, and wall thickness on their mechanical properties. Some optimal size combinations for the two structures, namely hollow unit block and grid unit block, were given based on the multivariate analysis of variance. To explore the potential transparent layer for PV pavements, Li et al. (2021) assessed the feasibility of waste tempered glass as the aggregates in transparent concrete. The results showed that the light transmittance of transparent concrete could be impacted by the waste tempered glass particle size and gradation, and cement amount and embedding degree between aggregates mainly affect the compressive strength. Besides, it has been proved by some researchers (Efthymiou et al., 2016; Xie and Wang, 2021) that PIPV modules are effective for mitigating the urban heat island (UHI) effect.

The PIST module, also known as pavement solar collector (PSC) or asphalt solar collector (ASC), can generate thermal energy as a combination of the conventional asphalt pavement and the solar thermal module. Many studies have been conducted to investigate the influence of various factors on the thermal performance of the PIST module, including glazing (Farzan et al., 2020; Farzan et al., 2021), pipe configurations (Zaim et al., 2020), albedo (Johnsson and Adl-Zarrabi, 2020), fluid flow rate (Johnsson and Adl-Zarrabi, 2020; Masoumi et al., 2020), pipe spacing (Johnsson and Adl-Zarrabi, 2020), inlet water temperature (Masoumi et al., 2020), asphalt conductivity (Masoumi et al., 2020), asphalt absorptivity (Masoumi et al., 2020), urban form (Nasir et al., 2017) and building geometry (Nasir et al., 2015). Jiang et al. (2021) utilized carbon fibers with high axial thermal conductivity as directional heat-induced channels in asphalt mixtures. The results showed that these channels could significantly improve asphalt mixtures' directional thermal conductivity and improve the PIST module's thermal performance. Moreover, the PIST module can also be used for snow or ice melting and is usually called hydronic asphalt pavement (HAP) or hydronic heating pavement (HHP) in this application. In summer, solar energy is harvested by the PIST module and stored in seasonal thermal energy storage connected to the PIST module. In winter, the stored energy, as the only energy source, would be pumped back to the pipes in the PIST module to melt snow or ice at the road surface. For this type of snow melting system, both thermal performance (Mirzanamadi et al., 2018a, 2020; Mirzanamadi et al., 2018b; Zhao et al., 2021) and mechanical performance (Zhu et al., 2021) have been studied in recent years. Furthermore, the PIST system also shows the

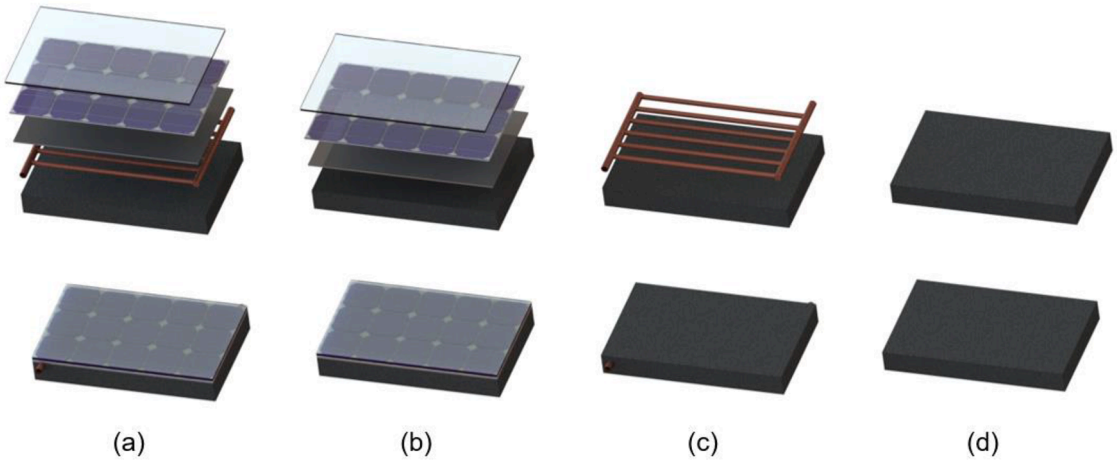

Fig. 1. Physical configurations of different solar energy harvesting pavements (a) PIPVT module; (b) PIPV module; (c) PIST module; (d) CP module

potential in mitigating the UHI effect (Nasir et al., 2020).

The PIPVT module is another emerging solar energy harvesting module. The PIPVT module can generate heat and electricity simultaneously since it is integrated with both PV cells and tubes. Hence, its overall energy efficiency could be very high, up to 3.95 times that of the PIPV module reported in the study of Xiang et al. (Xiang et al., 2020). Detailed parametric analysis has been performed in Ref. (Li et al., 2021; Xiang et al., 2020), showing the influence of various weather conditions and operating parameters on the PIPVT module's performance. According to a long-term performance simulation performed by Li et al. (2021), two PIPVT modules of 0.85 m^2 could generate 176.45 kWh heat and 125.04 kWh electricity annually in Shanghai, and the corresponding thermal, electrical, as well as PES efficiency were 18.03%, 12.78%, and 51.65%, respectively. Li et al. (2022) also studied the performance of the PIPVT system under three typical weather conditions and in five climatic regions, revealing that the PIPVT system performs well except on cloudy days with extremely low solar radiation that rarely appears. Besides, the highland climatic region is ideal for PIPVT application, with both the highest annual overall energy and exergy efficiencies of 37.89% and 14.17%, respectively.

Some studies focused on the performance analysis of the pavement modules in various weather conditions and in various urban form contexts. Llopis-Castelló et al. (2020) studied climate factors' influence, on pavement condition over time, finding that a cold Annual Average Temperature (5–15°C) and a large Annual Average Range of Temperature (20–30°C) could encourage a more aggressive pavement deterioration process, while warm climates with low temperature variations lead to a longer pavement service life. Nasir et al. (2017) investigated the urban form's influence on the performance of the road pavement solar collector with a tridimensional decoupled simulation approach based on weather conditions of June in Milan urban center, Italy. It was found that the road surface's temperature varied significantly in three different configurations. Besides, the road pavement solar collector system's performance degraded significantly when taller building row was behind the first approaching building row.

However, as indicated above, no existing research has so far focused on the influence of the PIPVT module on the UHI effect, a common phenomenon that the air temperature in metropolitan areas is significantly higher than that in surrounding suburban areas, which is very important to investigate the module's effect on urban microclimatic conditions and its adaptation in urban environments (Benrazavi et al., 2016; Jiang et al., 2019). Furthermore, most of the existing studies only concentrate on one type of solar energy harvesting pavement modules, while the detailed comparisons among all these different modules have not been conducted, which is essential to the overall understanding of solar energy harvesting pavement modules. Therefore, in this study, four typical days are selected to represent weather conditions in four seasons in Shanghai, and simulations are performed with validated mathematical models on the selected typical days. According to the simulated results, the operating performance and influence on the UHI effect of the PIPV module, PIST module, PIPVT module are assessed and compared, aiming to provide a clear view of the performance characteristics of various solar energy harvesting pavement modules and their differences in performance.

2. Configurations of different solar energy harvesting pavement modules

The configurations of different solar energy harvesting pavement modules are demonstrated in Fig. 1. The detailed structure of each module is exhibited in its cross-section in Fig. 2.

In the PIPVT module and PIPV module, the PV panel from Jinko

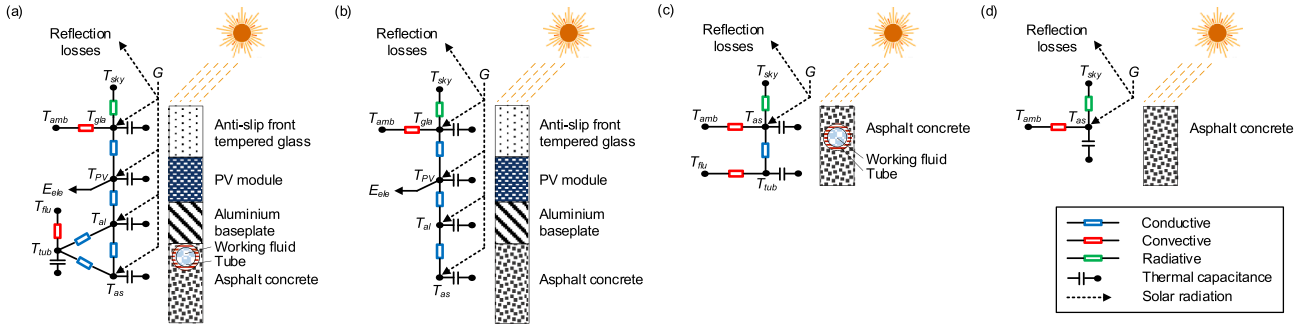

Fig. 2. . Thermal resistance networks of different solar energy harvesting pavements (a) PIPVT module; (b) PIPV module; (c) PIST module; (d) CP module

Table 1
Main parameters of pavement modules (Li et al., 2021; Li et al., 2022)

Parameters	Values
Maximum PV power	85.72 W
Nominal PV efficiency	20.17%
PV temperature coefficient	0.35%/C
Tube outer diameter	12 mm
Tube inner diameter	10 mm
Tube number	6
Tube spacing	8.33 mm
Length	0.85 m
Width	0.5 m
Slope	0°

Solar consists of 15 monocrystalline silicon solar cells. In the PIPVT module, six identical parallel copper tubes are surrounded by asphalt concrete and installed adjacent to the aluminum baseplate. In the PIST module, tubes are buried in the asphalt concrete. The tubes' buried depth of the PIST module is 27 mm, which is within its common range in the existing literature and equal to that of the PIPVT module. The main parameters of these modules are listed in Table 1.

3. Mathematical modeling and simulation

Two-dimensional transient models of different solar energy harvesting pavement modules were developed in this section in order to perform numerical simulations.

3.1. Thermophysical parameters and assumptions

The thermal and optical properties of the pavement modules' different layers are listed in Table 2.

Some assumptions are made in the numerical models for simplification, which are listed as follows:

- The heat transfer is negligible in the width direction, as shown in Fig. 1. The working fluid flow is uniform in each tube (Cai et al., 2017; Kazemian et al., 2019).
- The thermal and optical properties of each layer are constant and isotropic in each module (Ahmed et al., 2021b; Yu et al., 2019).
- Only the incident solar radiation is considered, while the influence of reflection from one layer to another is neglected (Gu et al., 2020; Gu et al., 2019).
- The PV efficiency is a function of temperature (Ahmed et al., 2021a; Kazemian et al., 2019).
- The thermal losses from the edge and bottom of the module are neglectable (Chen et al., 2011; Guldentops et al., 2016; Salari et al., 2020).

3.2. Energy balance equations

Energy transfer and conversion in different layers of each solar energy harvesting pavement module are shown in Fig. 2. As illustrated in Fig. 2(a), part of the solar energy reaching the PIPVT module's surface can penetrate the anti-slip front tempered glass and be converted into electricity by the PV module, while the majority of the incident solar energy is transformed into heat. Working fluid in the tubes can extract part of the generated heat away. As exhibited in Fig. 2(b), the energy transfer process in the PIPV module is similar to that in the PIPVT module due to their similar structures. The only difference is that the generated heat cannot be taken away since there is no tube or working fluid in the PIPV module. As shown in Fig. 2(c), most of the solar energy casting on the asphalt concrete is converted into heat that the working fluid can extract in tubes. As shown in Fig. 2(d), in the CP module, most of the incident solar energy is absorbed by the asphalt concrete and transformed into heat, which is stored in the asphalt concrete and increases its temperature.

The energy balance equations have been explained in detail in the

Table 3
Energy balance equations of PIPVT module

Study object	Energy balance equations
Anti-slip front tempered glass	$C_{gla}\delta_{gla}\rho_{gla}\frac{\partial T_{gla}}{\partial t} = \alpha_{gla}G - h_{v,gla-amb}(T_{gla}-T_{amb}) - h_{c,gla-PV}(T_{gla}-T_{PV})$ $-h_{r,gla-sky}(T_{gla}-T_{sky}) + k_{gla}\delta_{gla}\left(\frac{\partial^2 T_{gla}}{\partial x^2}+\frac{\partial^2 T_{gla}}{\partial y^2}\right)$ (1)
PV module	$C_{PV}\delta_{PV}\rho_{PV}\frac{\partial T_{PV}}{\partial t} = \tau_{gla}\alpha_{PV}G + h_{c,gla-PV}(T_{gla}-T_{PV}) - h_{c,PV-al}(T_{PV}-T_{al})$ $-\ddot{E}_{ele} + k_{PV}\delta_{PV}\left(\frac{\partial^2 T_{PV}}{\partial x^2}+\frac{\partial^2 T_{PV}}{\partial y^2}\right)$ (2) $\ddot{E}_{ele} = \tau_{gla}\alpha_{PV}G\eta_{ref}[1-\beta(T_{PV}-T_{ref})]$ (3)
Aluminum baseplate	$C_{al}\delta_{al}\rho_{al}\frac{\partial T_{al}}{\partial t} = \tau_{gla}\tau_{PV}\alpha_{al}G + h_{c,PV-al}(T_{PV}-T_{al})$ $-\frac{D_o}{W/N_{tub}}h_{c,al-tub}(T_{al}-T_{tub})$ $-h_{c,al-as}(T_{al}-T_{as}) + k_{al}\delta_{al}\left(\frac{\partial^2 T_{al}}{\partial x^2}+\frac{\partial^2 T_{al}}{\partial y^2}\right)$ (4)
Tubes	$\frac{\pi(D_o^2-D_i^2)}{4}C_{tub}\rho_{tub}\frac{\partial T_{tub}}{\partial t} = D_o h_{c,al-tub}(T_{al}-T_{tub})$ $-\left(1+\frac{\pi}{2}\right)D_o h_{c,tub-as}(T_{tub}-T_{as})$ $-\pi D_i h_{v,tub-flu}(T_{tub}-T_{flu})$ $+k_{tub}\frac{\pi(D_o^2-D_i^2)}{4}\left(\frac{\partial^2 T_{tub}}{\partial x^2}+\frac{\partial^2 T_{tub}}{\partial y^2}\right)$ (5)
Working fluid	$\frac{\pi D_i^2}{4}C_{flu}\rho_{flu}\frac{\partial T_{flu}}{\partial t} = \pi D_i h_{v,tub-flu}(T_{tub}-T_{flu}) - \frac{\pi D_i^2}{4}v_f\rho_{flu}C_{flu}\frac{\partial T_{flu}}{\partial y}$ (6)
Asphalt concrete	$C_{as}\rho_{as}\delta_{as}\frac{\partial T_{as}}{\partial t} = \frac{(1+\frac{\pi}{2})D_o}{W/N_{tub}}h_{c,tub-as}(T_{tub}-T_{as}) + h_{c,al-as}(T_{al}-T_{as})$ $+k_{as}\delta_{as}\left(\frac{\partial^2 T_{as}}{\partial x^2}+\frac{\partial^2 T_{as}}{\partial y^2}\right)$ (7)
Water mixing in the tank	$\rho_{flu}V_{flu,tank}c_{flu}\frac{\partial T_{flu,tank}}{\partial t} = \dot{m}_{flu}C_{flu}(T_{flu,tank,in}-T_{flu,tank})$ (8)

Table 2
Thermal and optical properties of pavement modules' different layers

Layers	Density	Thermal conductivity	Specific heat capacity	Absorptivity	Transmissivity	Emissivity	Thickness
	ρ (kg/m^3)	k (W/(m·K))	C (J/(kg·K))	α	τ	ε	δ (m)
Anti-slip front tempered glass (Xie and Wang, 2021)	3000	1.8	500	0.046	0.9	0.89	0.01
PV module (Kazemian et al., 2020; Li et al., 2021)	2330	140	900	0.90	0.06	-	0.006
Aluminum baseplate (Guo et al., 2015; Li et al., 2021; Sakellariou and Axaopoulos, 2018)	2770	237	910	0.95	0	-	0.005
Tubes (Li et al., 2020)	8920	377	386	-	-	-	0.001
Working fluid (Li et al., 2021)	996.95	0.61	4178.5	-	-	-	-
Asphalt concrete (Farzan et al., 2021; Masoumi et al., 2020)	2238	1.8	920	0.83	0	0.95	0.15

Table 4
Expressions of heat transfer coefficients

Category	Expression
Conductive(Duffie et al., 2020)	$h_{c,i-j} = \frac{1}{\frac{\delta_i}{2k_i}+\frac{\delta_j}{2k_j}}$(9)
Convective(Bejan, 2013; Li et al., 2018)	$h_{v,gla-amb} = 2.8 + 3.0v_{wind}$(10) $h_{v,tub-flu} = \frac{N_{u_f}\cdot k_f}{D_i}$(11) where $N_{u_f} = \begin{cases} 4.364, Re \le 2300 \\ 0.023Re^{0.8}Pr^{0.4}, Re > 2300 \end{cases}$
Radiative(Rejeb et al., 2015; Swinbank, 1963)	$h_{r,gla-sky} = \varepsilon_{gla}\sigma(T_{gla}^2+T_{sky}^2)(T_{gla}+T_{sky})$ (12) where $T_{sky} = 0.0552T_{amb}^{1.5}$

previous work (Li et al., 2021; Li et al., 2022). Thus, detailed explanations of the equations are not included in this section. Clear nomenclature has been listed in the beginning of this paper, which readers can refer to for better understanding of the equations in this section.

3.2.1. PIPVT module

According to the thermal resistance network of the PIPVT module in Fig. 2(a), energy balance equations employed in the model are given in Table 3. In the simulation, a water tank is connected with two PIPVT modules to form a system in which water circulates and is heated continuously. The energy balance in the water mixing process in the tank is also expressed as Eq. (8).

The expressions of various heat transfer coefficients in the above and following energy balance equations are listed in Table 4.

3.2.2. PIPV module

According to the thermal resistance network of the PIPV module in Fig. 2(b), energy balance equations employed in the model are given in Table 5.

3.2.3. PIST module

According to the thermal resistance network of the PIST module in Fig. 2(c), energy balance equations employed in the model are given in Table 6. In the simulation, a 50 L water tank is connected with two PIST modules to form a system in which water circulates and is heated continuously. The energy balance in the water mixing process in the tank is also expressed as Eq. (21).

3.2.4. CP module

According to the thermal resistance network of the CP module in Fig. 2(d), the energy balance equation employed in the model is given in Table 7.

Table 7
The energy balance equation of conventional pavement module

Study object	Energy balance equation
Asphalt concrete	$C_{as}\delta_{as}\rho_{as}\frac{\partial T_{as}}{\partial t} = \alpha_{as}G - h_{v,as-amb}(T_{as}-T_{amb}) - h_{r,as-sky}(T_{as}-T_{sky}) + k_{as}\delta_{as}\left(\frac{\partial^2 T_{as}}{\partial x^2}+\frac{\partial^2 T_{as}}{\partial y^2}\right)$ (22)

Table 5
Energy balance equations of PIPV module

Study object	Energy balance equations
Anti-slip front tempered glass	$C_{gla}\delta_{gla}\rho_{gla}\frac{\partial T_{gla}}{\partial t} = \alpha_{gla}G - h_{v,gla-amb}(T_{gla}-T_{amb}) - h_{c,gla-PV}(T_{gla}-T_{PV}) - h_{r,gla-sky}(T_{gla}-T_{sky}) + k_{gla}\delta_{gla}\left(\frac{\partial^2 T_{gla}}{\partial x^2}+\frac{\partial^2 T_{gla}}{\partial y^2}\right)$ (13)
PV module	$C_{PV}\delta_{PV}\rho_{PV}\frac{\partial T_{PV}}{\partial t} = \tau_{gla}\alpha_{PV}G + h_{c,gla-PV}(T_{gla}-T_{PV}) - h_{c,PV-al}(T_{PV}-T_{al}) - \ddot{E}_{ele} + k_{PV}\delta_{PV}\left(\frac{\partial^2 T_{PV}}{\partial x^2}+\frac{\partial^2 T_{PV}}{\partial y^2}\right)$ (14)
$\ddot{E}_{ele} = \tau_{gla}\alpha_{PV}G\eta_{ref}[1-\beta(T_{PV}-T_{ref})]$	(15)
Aluminum baseplate	$C_{al}\delta_{al}\rho_{al}\frac{\partial T_{al}}{\partial t} = \tau_{gla}\tau_{PV}\alpha_{al}G + h_{c,PV-al}(T_{PV}-T_{al}) - h_{c,al-as}(T_{al}-T_{as}) + k_{al}\delta_{al}\left(\frac{\partial^2 T_{al}}{\partial x^2}+\frac{\partial^2 T_{al}}{\partial y^2}\right)$ (16)
Asphalt concrete	$C_{as}\rho_{as}\delta_{as}\frac{\partial T_{as}}{\partial t} = h_{c,al-as}(T_{al}-T_{as}) + k_{as}\delta_{as}\left(\frac{\partial^2 T_{as}}{\partial x^2}+\frac{\partial^2 T_{as}}{\partial y^2}\right)$ (17)

Table 6
Energy balance equations of PIST module

Study object	Energy balance equations
Asphalt concrete	$C_{as}\rho_{as}\delta_{as}\frac{\partial T_{as}}{\partial t} = \alpha_{as}G - \frac{\pi D_o}{W/N_{tub}}h_{c,as-tub}(T_{as}-T_{tub}) - h_{v,as-amb}(T_{as}-T_{amb}) - h_{r,as-sky}(T_{as}-T_{sky}) + k_{as}\delta_{as}\left(\frac{\partial^2 T_{as}}{\partial x^2}+\frac{\partial^2 T_{as}}{\partial y^2}\right)$ (18)
Tubes	$\frac{\pi(D_o^2-D_i^2)}{4}C_{tub}\rho_{tub}\frac{\partial T_{tub}}{\partial t} = \pi D_o h_{c,as-tub}(T_{as}-T_{tub}) - \pi D_i h_{v,tub-flu}(T_{tub}-T_{flu}) + k_{tub}\frac{\pi(D_o^2-D_i^2)}{4}\left(\frac{\partial^2 T_{tub}}{\partial x^2}+\frac{\partial^2 T_{tub}}{\partial y^2}\right)$ (19)
Working fluid	$\frac{\pi D_i^2}{4}C_{flu}\rho_{flu}\frac{\partial T_{flu}}{\partial t} = \pi D_i h_{v,tub-flu}(T_{tub}-T_{flu}) - \frac{\pi D_i^2}{4}v_f\rho_{flu}C_{flu}\frac{\partial T_{flu}}{\partial y}$ (20)
Water mixing in the tank	$\rho_{flu}V_{flu,tank}c_{flu}\frac{\partial T_{flu,tank}}{\partial t} = \dot{m}_{flu}C_{flu}(T_{flu,tank,in}-T_{flu,tank})$ (21)

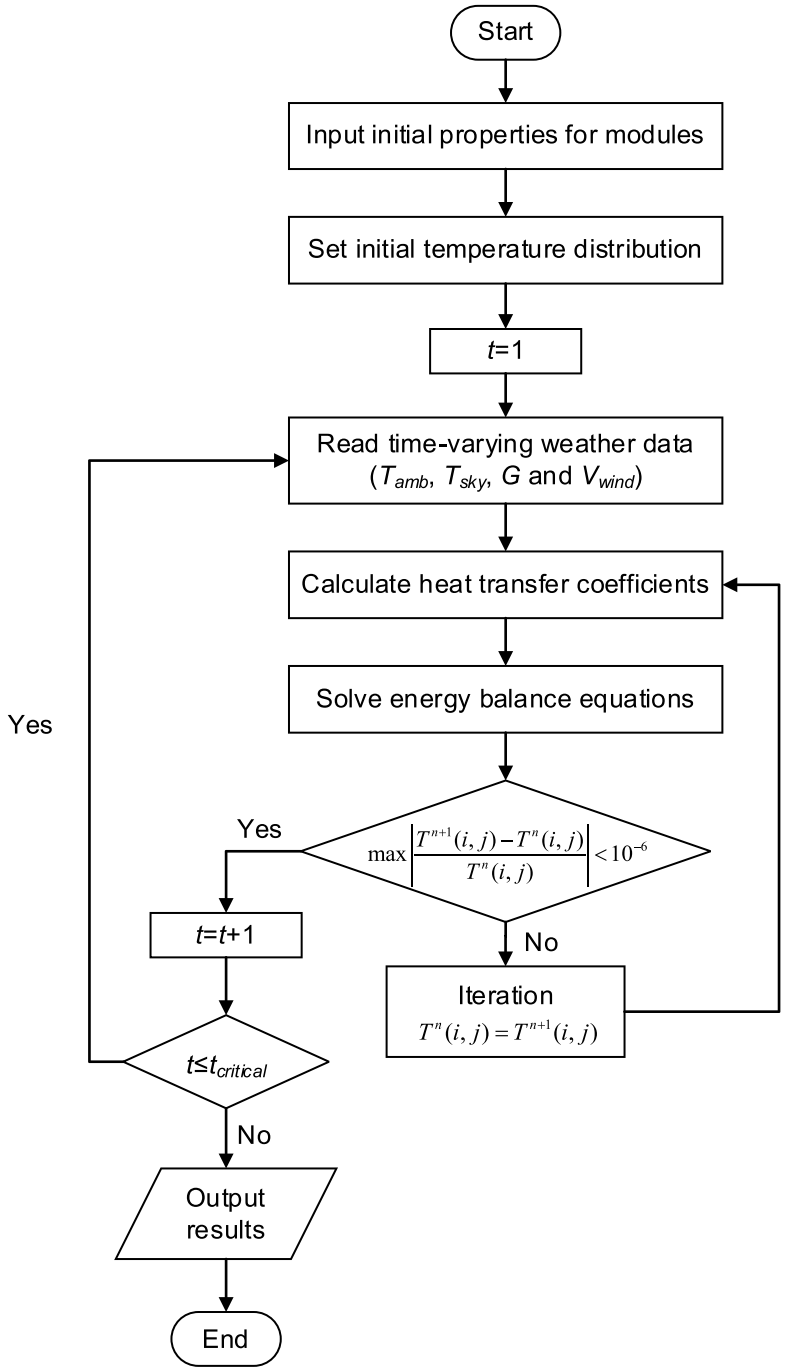

Fig. 3. Flow chart of the numerical simulation procedure

3.3. Numerical simulation procedure

The procedure of the numerical simulation conducted in MATLAB is shown in Fig. 3. First, the optical parameters and thermophysical parameters are input into the simulation program as the initial properties. Besides, the initial temperature distribution of the system is set. Subsequently, the time-varying weather data measured on the horizontal surface in Shanghai is read. Next, the energy balance equations are solved with the calculated heat transfer coefficients. In each timestep, the iteration will stop only if the convergence value is less than 10^{-6}. Finally, when t is greater than $t_{critical}$, the iteration ceases, and the results are given out. In the simulation of each case, the system operates from 8:00 to 16:00.

3.4. Performance evaluation criteria

3.4.1. Evaluation methods of simulated results

To examine the feasibility of the developed models in this study, the relative error (RE) and root mean square deviation (RMSD) are employed for the comparisons between experimental and numerical results, defined as:

$$RE = \frac{R_{sim,i} - R_{exp,i}}{R_{exp,i}} \times 100\% \tag{23}$$

$$RMSD = \sqrt{\frac{\sum\left[\left(R_{sim,i} - R_{exp,i}\right)/\left(R_{exp,i}\right)\right]^2}{N_{exp}}} \times 100\% \tag{24}$$

where $R_{exp,i}$ and $R_{sim,i}$ are the experimental and simulated results at point i, respectively, and N_{exp} is the number of experimental points.

3.4.2. Indicators of energy generation

To assess the energy generation performance of different solar energy harvesting pavement modules, electrical efficiency η_{ele}, thermal efficiency η_{th}, and overall efficiency η_{all} are employed in this paper.

For the PIPVT module and PIPV module that can generate electricity, electrical efficiency is introduced to indicate their electrical performance. Electrical efficiency is defined as Rekioua and Matagne (2012):

$$\eta_{ele} = \frac{\dot{E}_{ele}}{\dot{E}_{sun}} \tag{25}$$

where $\dot{E}_{sun}$is the incident solar power and $\dot{E}_{ele}$ is the generated electrical power, denoted by:

$$\dot{E}_{sun} = A_c G \tag{26}$$

$$\dot{E}_{ele} = A_c \alpha_{PV,e} G \eta_{ref} \left[1 - \beta\left(T_{PV} - T_{ref}\right)\right] \tag{27}$$

For the PIPVT module and PIST module that can generate heat, thermal efficiency is introduced to indicate their thermal performance. Corresponding to the definition of electrical efficiency, the thermal efficiency is defined as:

$$\eta_{th} = \frac{\dot{E}_{th}}{\dot{E}_{sun}} \tag{28}$$

where $\dot{E}_{th}$ is the generated thermal power, derived as:

$$\dot{E}_{th} = c_{flu}\rho_{flu}V_{flu,tank}\frac{\partial T_{flu,tank}}{\partial t} \tag{29}$$

Specially for the PIPVT module that can generate electrical and thermal energy simultaneously, the overall energy efficiency is introduced to indicate its overall performance, which is defined as the sum of the thermal and electrical energy efficiency:

$$\eta_{all} = \eta_{th} + \eta_{ele} \tag{30}$$

3.4.3. Indicators of the UHI effect

UHI effect is a phenomenon that the air temperature in urban areas is higher than that in surrounding rural areas, which can be attributed to the heat output caused by human activities. (Elqattan and Elrayies, 2021; Tian et al., 2021) Hence, when it comes to the pavements' impact on the UHI effect, heat output intensity from the pavement surface to the ambient environment would be a direct and significant indicator. Given the heat exchange processes on the pavement surface (Nwakaire et al., 2020), including the emitted radiation (long-wave radiation), the reflection of solar radiation (short-wave radiation), and the convective heat transfer, heat output intensity from pavement surface can be calculated as:

$$\ddot{E}_{th,out} = h_{r,sur-sky}\left(T_{sur} - T_{sky}\right) + h_{v,sur-amb}\left(T_{sur} - T_{amb}\right) + \ddot{E}_{rfl} \tag{31}$$

where $\ddot{E}_{rfl}$ is the reflected solar radiation. $\ddot{E}_{rfl}$ varies in different pavements because of their different structures. In PIST module and conventional pavement module, $\ddot{E}_{rfl}$ can be expressed as:

$$\ddot{E}_{rfl} = \gamma_{as} G \tag{32}$$

In PIPVT and PIPV modules, anti-slip front tempered glass is transparent. Therefore, in addition to the reflection on the anti-slip front tempered glass, the PV module can also reflect the solar radiation penetrating the glass. Correspondingly, $\ddot{E}_{rfl}$ is composed of two parts, which can be written as:

$$\ddot{E}_{rfl} = \gamma_{gla} G + \tau_{gla}\gamma_{PV}\left(1 - \alpha_{gla}\right)G \tag{33}$$

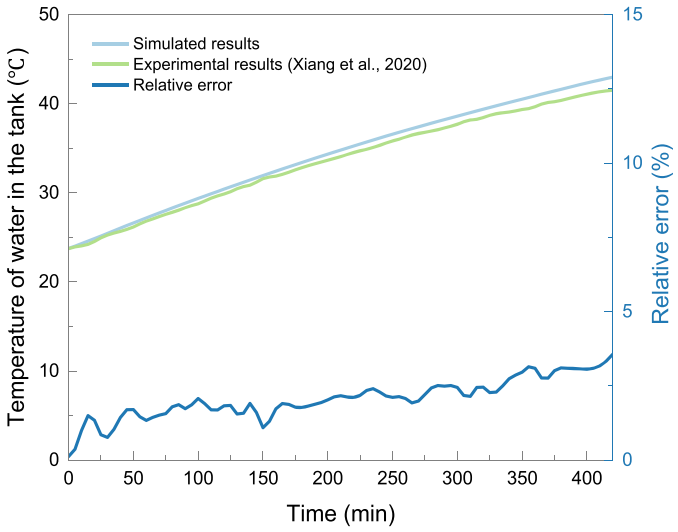

Fig. 4. Comparisons between experimental results (Xiang et al., 2020) and simulated results of PIPVT modules

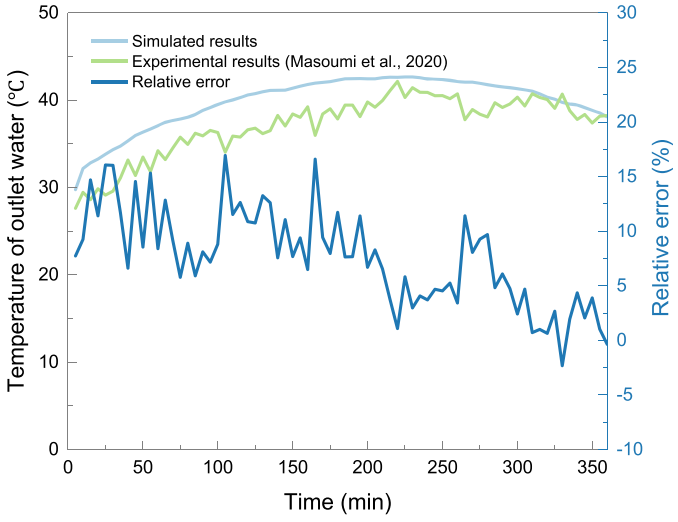

Fig. 5. Comparisons between experimental results (Masoumi et al., 2020) and simulated results of PIST modules

In theory, a very small part of the solar radiation reflected by the PV module would be reflected again by the anti-slip front tempered glass. Since this part is so small that it has little effect on the overall heat output, it is assumed that part of the solar radiation reflected by the PV module would be absorbed by anti-slip front tempered glass and the rest penetrates the glass to the ambient environment without any reflections.

In addition to heat output intensity from the pavement surface, the other indicator of the UHI effect employed in this study is pavement surface temperatureT_{sur}, which is defined as the average of simulated points' temperatures on the pavement surface. Since the pavement surface with a higher temperature has more potential to transfer heat to the ambient environment through the convective and radiative process, its temperature is also an important factor to indicate the module's impact on the UHI effect.

4. Results and discussions

4.1. Validation

For validation, the simulations are conducted for both PIPVT

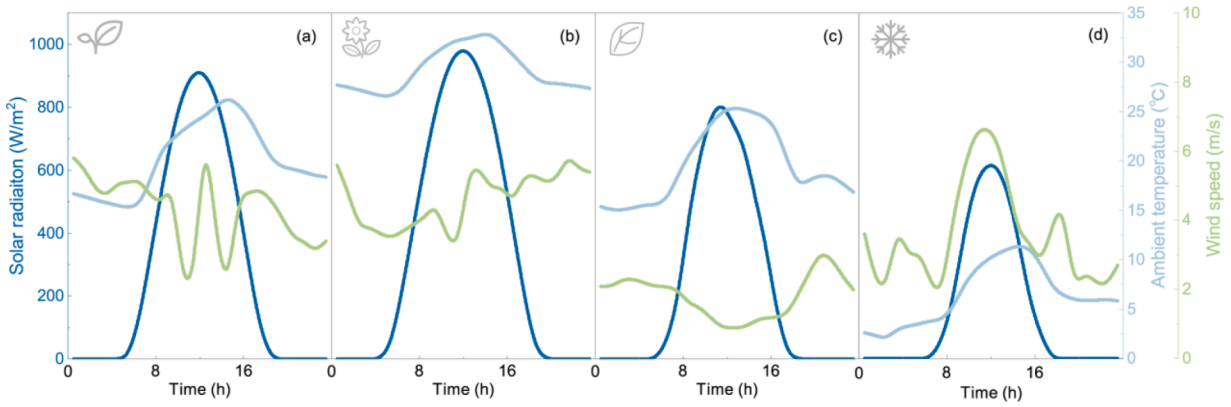

Fig. 6. Weather conditions on four typical sunny days (a) 10th Apr. (spring); (b) 14th Jul. (summer); (c) 2nd Oct. (autumn); (d) 14th Jan. (winter)

modules and PIST modules using the developed mathematical models. Both design parameters and operating parameters in the simulations are kept consistent with those in the experiments (Masoumi et al., 2020; Xiang et al., 2020). As shown in Fig. 4 and Fig. 5, the simulated results are compared with experimental results for PIPVT modules and PIST modules, respectively.

As illustrated in Fig. 4, for PIPVT modules, the simulated results exhibit very good agreement with experimental results. RE ranges from 0.12% to 3.57%, and RMSD is 2.18%, which might be attributed to the error of measurement devices and the simplified assumptions of the model. The above results indicate that the mathematical model of PIPVT modules is feasible and could be employed for performance assessment.

For PIST modules, as shown in Fig. 5, the simulated results have a consistent trend with experimental results. The simplification of mathematical models and the accuracy of measurement equipment could affect the deviations. Hence, considering the above factors, RE ranging from –2.32 % to 16.94 % and RMSD of 8.79 % are acceptable.

Overall, it is believed that the proposed models can be used to predict the performance of typical solar energy harvesting pavement modules with adequate accuracy.

4.2. Performance simulation and assessment

Four typical days representing four seasons were selected for simulations to investigate the operating performance of solar energy harvesting pavements in different seasons. As shown in Fig. 6, four selected typical days are all sunny with stable solar radiation, while both the magnitudes of solar radiation and ambient temperature vary in four seasons. All the weather conditions were measured at the campus of Shanghai Jiao Tong University in Shanghai, China (31.17 °N / 121.43 °E). The above weather data for the typical spring, summer, autumn, and winter days was recorded on 10th April, 14th July, 2nd October, 14th January in 2018, respectively. In the case of each typical day, energy yield, energy efficiency, maximum asphalt temperature, and maximum temperature of water in the tank are studied as operating performance indicators. For the PIPVT and PIST modules that have working fluid inside the tubes, a corresponding water circulation system would be set up with the integration of a water tank. Reference to the parametric analysis conducted in the previous study (Li et al., 2021), the water flow rate for each tube and the volume of the water tank were set as 0.04 kg/s and 50 L, respectively. In each case, two identical modules connected in series are employed to conduct simulations, and the system operates from 8:00 to 16:00.

With flowing water that can extract the heat continuously, the temperature of PV cells in the PIPVT module is lower than that in the PIPV module. Therefore, as shown in Fig. 7, the electrical efficiency of the former is higher than that of the latter on each day. Correspondingly, the electricity yield of the PIPVT module is 2.78%, 2.56%, 3.37% and 1.39% higher than that of the PIPV module on spring, summer, autumn and winter days, respectively. Specifically, the PIPVT module can output 0.96 kWh/m^2, 1.02 kWh/m^2, 0.81 kWh/m^2 and 0.59 kWh/m^2 electricity on spring, summer, autumn and winter days, respectively.

In the PIPVT module, the absorbed solar radiation is transformed into electricity and heat simultaneously. Compared with the PIST module that only focuses on heat generation, the PIPVT module has relatively lower thermal efficiency. The heat yield of the PIPVT module is in the range from 15.80% to 23.87%, which is lower than that of the PIST module. Specifically, the PIPVT module can output 1.29 kWh/m^2, 1.25 kWh/m^2, 1.19 kWh/m^2 and 0.71 kWh/m^2 heat on spring, summer, autumn and winter days, respectively. When considering both electricity

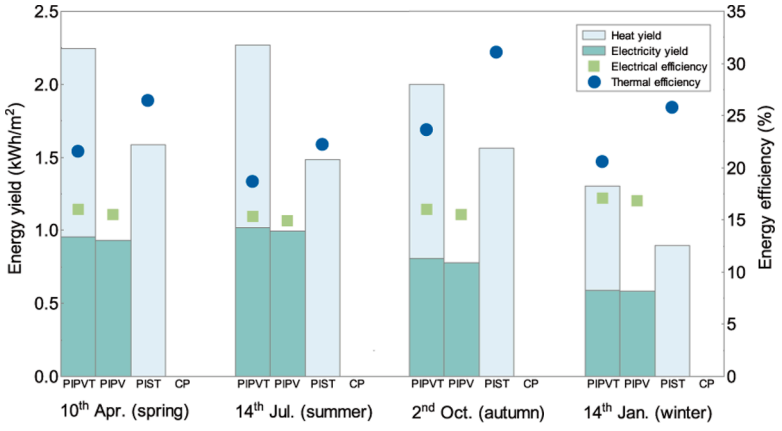

Fig. 7. Energy yield and efficiency of solar energy harvesting pavements on four typical days

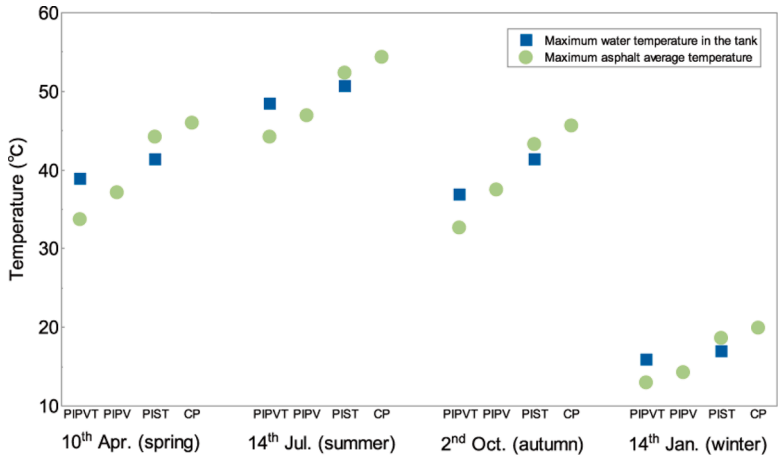

Fig. 8. Maximum water and asphalt temperatures of solar energy harvesting pavements on four typical days

and heat yields, the PIPVT module can achieve the average overall energy efficiency of 37.31%.

The above results demonstrate that the electrical efficiency is impacted apparently by solar radiation and ambient temperature. When solar radiation increases, more solar energy penetrates the anti-slip front tempered glass and is converted into heat on the PV module. Therefore, the temperature of the PV module will be higher, which causes lower electrical efficiency. Additionally, the higher ambient temperature will lead to a smaller temperature difference between the module's surface and ambient temperature, thus weakening the convective heat transfer and increasing the temperature of the PV module. The increased PV temperature results in lower electrical efficiency. Therefore, both the PIPVT module and the PIPV module have the lowest electrical efficiency on the summer day that has the highest solar radiation and the highest ambient temperature simultaneously. Similarly, the highest electrical efficiency can be observed on the winter day with both the lowest solar radiation and the lowest ambient temperature. Despite the lowest electrical efficiency, both the PIPVT module and the PIPV module generate the most electricity on the summer day because the solar radiation is much higher than any other typical day. Similarly, the least electricity yield appears on the winter day, although it has the highest electrical efficiency.

Notably, for both PIPVT and PIST modules, the lowest thermal efficiencies are observed on the typical summer day, which is attributed to the intensive solar radiation, high ambient temperature as well as limited water tank volume. In all cases, the initial water temperature is set as the same value as the ambient temperature when the system begins operating. As illustrated in Fig. 6, the ambient temperature and thus the initial water temperature on the summer day are much higher than those on any other day. According to the simulated results, the temperatures of the module and circulating water increase rapidly at the beginning with intensive solar radiation. Thus, the temperature difference between the module and the ambient increases, enhancing the convective and radiative losses. Subsequently, the results show that the water temperature increases very slowly, and most of the incident solar energy is dissipated to the environment. Therefore, the thermal efficiency is lowest on the summer day even though the solar radiation is highest. According to the above analysis and Ref. (Li et al., 2021), enlarging the water volume could be an effective measure to increase the thermal efficiency and heat yield in summer because the water temperature would not increase so rapidly with more circulating water. It should be noted that the selected typical days are all entirely sunny days with intensive and stable solar radiation, which may not usually appear in each corresponding season. Therefore, in the previous study (Li et al., 2021), the highest seasonal overall thermal efficiency of the PIPVT module in Shanghai is still observed in summer, even though the lowest thermal efficiency appears on the typical summer day in this study.

For both PIPVT and PIST modules, the heat yield is abundant and stable on spring, summer, and autumn days, while significantly less on the typical winter day with both the lowest solar radiation and ambient temperature. Besides, it could be expected that the modules will have diverse operating performances in different climatic regions with different weather conditions, such as in temperate monsoon climatic region, tropical monsoon climatic region and so on Li et al. (2021).

In addition to the energy yield and efficiency, the water temperature in the tank is also studied to indicate the operating performance of different solar energy harvesting pavement modules, as shown in Fig. 8. Consistent with the above-mentioned results of heat yield, the maximum water temperature in the tank of the PIPVT system is 2.41°C, 2.25°C, 4.49°C and 1.06°C lower than that of PIST system on spring, summer, autumn and winter days, respectively. For both PIPVT and PIST modules, the highest and the lowest maximum water temperature in the tank are obtained on summer and winter days, respectively. This result could be ascribed to the highest solar radiation and ambient temperature on the typical summer day, as well as the lowest ones on the typical winter day. The PIPVT module can increase the water temperature to 38.90°C, 48.39°C, 36.92°C and 15.94°C on spring, summer, autumn and winter days, respectively. The maximum water temperatures of the PIST system are 41.31°C, 50.65°C, 41.41°C and 17.00°C on spring, summer, autumn and winter days, respectively. The results reveal that both the PIPVT and PIST modules are capable of generating hot water whose temperature is high enough for domestic use, such as bath on spring, summer and autumn days. Neither the PIPVT module nor PIST module can generate water hot enough for domestic use on the typical winter day, indicating that an auxiliary heater would be necessary, while these modules could only be utilized to preheat the water for domestic water heating in winter.

Asphalt temperature is another considered factor in this study since high temperature could accelerate the thermal aging of asphalt concrete (Menapace et al., 2017). Besides, the high temperature of asphalt concrete could also exacerbate pavement rutting when the pavement surface is made of asphalt concrete (Du et al., 2020). Fig. 8 exhibits the maximum asphalt average temperatures of different solar energy harvesting pavement modules on four typical days. All three solar energy harvesting pavement modules have lower maximum asphalt average temperatures than the conventional pavement module. The PIPVT module can convert the incident solar energy into electricity and heat simultaneously, which utilizes the solar energy most thoroughly among the three solar energy harvesting pavement modules investigated in this study. Hence, the PIPVT module stores the least energy in the asphalt concrete. Consequently, the PIPVT module has the most significant effect on the reduction of the maximum asphalt average temperature,

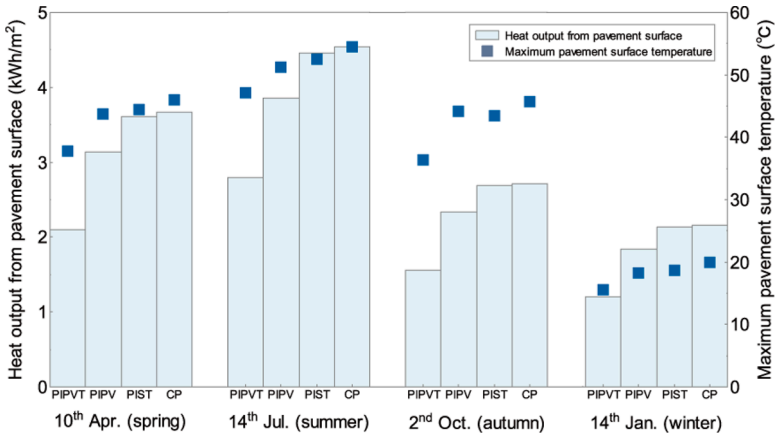

Fig. 9. Heat output from pavement surface and maximum pavement surface temperature of solar energy harvesting pavements on four typical days

decreasing it by 12.26°C, 10.12°C, 12.96°C and 6.94°C on spring, summer, autumn and winter days, respectively, compared to the CP module.

4.3. Influence on the UHI effect

In this section, all the conditions and settings are the same as these in Section 4.2. Heat output from pavement surface and maximum pavement surface temperature are employed to indicate the solar energy harvesting pavement modules' influence on the UHI effect. As exhibited in Fig. 9, the PIPVT module outputs the least energy from the pavement surface and correspondingly has the lowest temperature on all typical days, revealing that it has the most significant influence on the mitigation of the UHI effect. Specifically, in comparison with the CP module, the PIPVT module can reduce the heat output from pavement surface by 42.78%, 38.48%, 42.83%, and 43.96% on spring, summer, autumn, and winter days, respectively. In addition, it can also reduce the maximum pavement surface temperature by 8.23°C, 7.30°C, 9.37°C and 4.48°C on spring, summer, autumn and winter days, respectively.

Besides the PIPVT module, the PIPV module can also apparently mitigate the UHI effect on all typical days since its heat output from the pavement surface and maximum pavement surface temperature are both less than those of the CP module. However, according to the above two indicators, the PIST module only has a very slight influence on the UHI effect mitigation.

The above results indicate that the installation of PIPVT modules and PIPV modules could be an effective method to mitigate the UHI effect and improve the urban microclimate in addition to the application of cool pavements, which are made of cool materials with higher solar reflectance and infrared emittance compared to conventional paving materials (Kolokotsa et al., 2018; Tsoka et al., 2018).

5. Conclusions

In this study, two-dimensional transient models were developed and validated for three typical solar energy harvesting pavement modules, namely, pavement-integrated photovoltaic (PIPV) module, pavement-integrated solar thermal (PIST) module, and pavement-integrated photovoltaic thermal (PIPVT) module. To investigate and compare the performance of these modules, simulations were conducted with the developed mathematical models on the weather conditions of four typical days representing four seasons in Shanghai.

The electricity yield of the PIPVT module is slightly higher than that of the PIPV module, while its heat yield is lower than that of the PIST module on all typical days. When considering both electricity and heat yields, the PIPVT module can achieve the average overall energy efficiency of 37.31%.

The PIST module can output hotter water than the PIPVT module on all typical days. Neither the PIPVT module nor PIST module can heat water to adequate temperature for domestic use on the typical winter day, indicating that an auxiliary heater would be necessary, while the modules could only be utilized to preheat the water for domestic water heating in winter.

Compared with the conventional pavement (CP) module, all three solar energy harvesting pavement modules have lower maximum asphalt average temperatures that can decelerate the thermal aging of asphalt concrete. The PIPVT module has the most significant effect on the reduction of the maximum asphalt average temperature, decreasing it by 10.57°C on average.

All three solar energy harvesting pavement modules can mitigate the urban heat island (UHI) effect, indicating that the installation of solar energy harvesting pavements can improve the urban microclimate. The PIPVT module has the most significant influence on UHI effect mitigation with the least heat output from pavement surface and correspondingly the lowest maximum pavement surface temperature on all typical days. Specifically, in comparison with the CP module, the PIPVT module can reduce the heat output from pavement surface and the maximum pavement surface temperature by 42.01% and 7.35°C on average, respectively. However, the influence on UHI effect mitigation of the PIST module is very slight.

Declaration of Competing Interest

The authors declare that they have no known competing financial interests or personal relationships that could have appeared to influence the work reported in this paper.

Acknowledgment

The authors would appreciate the financial supports provided by National Natural Science Foundation of China (Grant No. 51976124), National Key Research and Development Program of China (Grant No. 2019YFE0104900), the Zhejiang Provincial Natural Science Foundation (Grant No. LR20E060001), and the State Key Laboratory of Clean Energy utilization (Grant No. ZJUCEU2020006).

References

Ahmed, S., Li, Z., Javed, M. S., & Ma, T. (2021a). A review on the integration of radiative cooling and solar energy harvesting. *Materials Today Energy*.

Ahmed, S., Li, Z., Ma, T., Javed, M. S., & Yang, H. (2021b). A comparative performance evaluation and sensitivity analysis of a photovoltaic-thermal system with radiative cooling. *Solar Energy Materials and Solar Cells, 221*.

Bejan, A. (2013). *Convection heat transfer*. John wiley & sons.

Benrazavi, R. S., Binti Dola, K., Ujang, N., & Sadat Benrazavi, N. (2016). Effect of pavement materials on surface temperatures in tropical environment. *Sustainable Cities and Society, 22*, 94–103.

Cai, J., Ji, J., Wang, Y., Zhou, F., & Yu, B. (2017). A novel PV/T-air dual source heat pump water heater system: Dynamic simulation and performance characterization. *Energy Conversion and Management, 148*, 635–645.

Chen, M., Wu, S., Wang, H., & Zhang, J. (2011). Study of ice and snow melting process on conductive asphalt solar collector. *Solar Energy Materials and Solar Cells, 95*(12), 3241–3250.

Du, Y., Dai, M., Deng, H., Deng, D., Wei, T., & Li, W. (2020). Evaluation of thermal and anti-rutting behaviors of thermal resistance asphalt pavement with glass microsphere. *Construction and Building Materials, 263*.

Duffie, J. A., Beckman, W. A., & Blair, N. (2020). *Solar engineering of thermal processes, photovoltaics and wind*. John Wiley & Sons.

Efthymiou, C., Santamouris, M., Kolokotsa, D., & Koras, A. (2016). Development and testing of photovoltaic pavement for heat island mitigation. *Solar Energy, 130*, 148–160.

Elqattan, A. A., & Elrayies, G. M. (2021). Developing a novel solar-driven cool pavement to improve the urban microclimate. *Sustainable Cities and Society, 64*.

Farzan, H., Zaim, E. H., & Ameri, M. (2020). Study on effect of glazing on performance and heat dynamics of asphalt solar collectors: An experimental study. *Solar Energy, 202*, 429–437.

Farzan, H., Zaim, E. H., Ameri, M., & Amiri, T. (2021). Study on effects of wind velocity on thermal efficiency and heat dynamics of pavement solar collectors: An experimental and numerical study. *Renewable Energy, 163*, 1718–1728.

Gu, W., Ma, T., Li, M., Shen, L., & Zhang, Y. (2020). A coupled optical-electrical-thermal model of the bifacial photovoltaic module. *Applied Energy*, 258.

Gu, W., Ma, T., Shen, L., Li, M., Zhang, Y., Zhang, W., 2019. Coupled electrical-thermal modelling of photovoltaic modules under dynamic conditions. Energy 188.

Guldentops, G., Nejad, A. M., Vuye, C., Van den bergh, W., & Rahbar, N. (2016). Performance of a pavement solar energy collector: Model development and validation. *Applied Energy, 163*, 180–189.

Guo, C., Ji, J., Sun, W., Ma, J., He, W., & Wang, Y. (2015). Numerical simulation and experimental validation of tri-functional photovoltaic/thermal solar collector. *Energy, 87*, 470–480.

Javed, M. S., Ma, T., Jurasz, J., Canales, F. A., Lin, S., Ahmed, S., & Zhang, Y. (2021). Economic analysis and optimization of a renewable energy based power supply system with different energy storages for a remote island. *Renewable Energy, 164*, 1376–1394.

Javed, M. S., Song, A., & Ma, T. (2019). Techno-economic assessment of a stand-alone hybrid solar-wind-battery system for a remote island using genetic algorithm. *Energy, 176*, 704–717.

Jiang, J., Jin, Y., Bao, T., & Ou, X. (2019). Sensible heat discharging from pavements with varying thermophysical properties. *Sustainable Cities and Society, 45*, 431–438.

Jiang, L., Wang, S., Gu, X., Dorjee, N., & Bo, W. (2021). Inducing directional heat transfer by enhancing directional thermal conductivity of asphalt mixtures for improving asphalt solar collectors. *Construction and Building Materials, 267*.

Johnsson, J., & Adl-Zarrabi, B. (2020). A numerical and experimental study of a pavement solar collector for the northern hemisphere. *Applied Energy*, 260.

Kazemian, A., Salari, A., Hakkaki-Fard, A., & Ma, T. (2019). Numerical investigation and parametric analysis of a photovoltaic thermal system integrated with phase change material. *Applied Energy, 238*, 734–746.

Kazemian, A., Salari, A., & Ma, T. (2020). A year-round study of a photovoltaic thermal system integrated with phase change material in Shanghai using transient model. *Energy Conversion and Management, 210*.

Kolokotsa, D. D., Giannariakis, G., Gobakis, K., Giannarakis, G., Synnefa, A., & Santamouris, M. (2018). Cool roofs and cool pavements application in Acharnes. *Greece. Sustainable Cities and Society, 37*, 466–474.

Li, J., Ren, X., Yuan, W., Li, Z., Pei, G., Su, Y., Kutlu, Ç., Ji, J., & Riffat, S. (2018). Experimental study on a novel photovoltaic thermal system using amorphous silicon cells deposited on stainless steel. *Energy, 159*, 786–798.

Li, M., Zhong, D., Ma, T., Kazemian, A., & Gu, W. (2020). Photovoltaic thermal module and solar thermal collector connected in series: Energy and exergy analysis. *Energy Conversion and Management, 206*, Article 112479.

Li, S., Chen, Z., Liu, X., Zhang, X., Zhou, Y., Gu, W., & Ma, T. (2021). Numerical simulation of a novel pavement integrated photovoltaic thermal (PIPVT) module. *Applied Energy, 283*, Article 116287.

Li, S., Gu, W., Liu, X., Zhou, Y., Chen, Z., Zhang, X., & Ma, T. (2022). Pavement integrated photovoltaic thermal (PIPVT) system: A temporal and spatial analysis of energy and exergy performance. *Journal of Cleaner Production, 340*, Article 130782.

Liu, Z., Yang, A., Gao, M., Jiang, H., Kang, Y., Zhang, F., & Fei, T. (2019). Towards feasibility of photovoltaic road for urban traffic-solar energy estimation using street view image. *Journal of Cleaner Production, 228*, 303–318.

Llopis-Castelló, D., García-Segura, T., Montalbán-Domingo, L., Sanz-Benlloch, A., & Pellicer, E. (2020). Influence of Pavement Structure. *Traffic, and Weather on Urban Flexible Pavement Deterioration. Sustainability, 12*(22).

Ma, T., Yang, H., Gu, W., Li, Z., & Yan, S. (2019). Development of walkable photovoltaic floor tiles used for pavement. *Energy Conversion and Management, 183*, 764–771.

Ma, T., Yang, H., & Lu, L. (2014). Development of a model to simulate the performance characteristics of crystalline silicon photovoltaic modules/strings/arrays. *Solar Energy, 100*(0), 31–41.

Ma, T., Yang, H., & Lu, L. (2015). Development of hybrid battery–supercapacitor energy storage for remote area renewable energy systems. *Applied Energy(0)*.

Masoumi, A. P., Tajalli-Ardekani, E., & Golneshan, A. A. (2020). Investigation on performance of an asphalt solar collector: CFD analysis, experimental validation and neural network modeling. *Solar Energy, 207*, 703–719.

Menapace, I., Yiming, W., & Masad, E. (2017). Chemical analysis of surface and bulk of asphalt binders aged with accelerated weathering tester and standard aging methods. *Fuel, 202*, 366–379.

Mirzanamadi, R., Hagentoft, C.-E., & Johansson, P. (2018a). An analysis of hydronic heating pavement to optimize the required energy for anti-icing. *Applied Thermal Engineering, 144*, 278–290.

Mirzanamadi, R., Hagentoft, C.-E., & Johansson, P. (2020). Coupling a Hydronic Heating Pavement to a Horizontal Ground Heat Exchanger for harvesting solar energy and heating road surfaces. *Renewable Energy, 147*, 447–463.

Mirzanamadi, R., Hagentoft, C.-E., Johansson, P., & Johnsson, J. (2018b). Anti-icing of road surfaces using Hydronic Heating Pavement with low temperature. *Cold Regions Science and Technology, 145*, 106–118.

Nasir, D. S. N. M., Hughes, B. R., & Calautit, J. K. (2015). A study of the impact of building geometry on the thermal performance of road pavement solar collectors. *Energy, 93*, 2614–2630.

Nasir, D. S. N. M., Hughes, B. R., & Calautit, J. K. (2017). Influence of urban form on the performance of road pavement solar collector system: Symmetrical and asymmetrical heights. *Energy Conversion and Management, 149*, 904–917.

Nasir, D. S. N. M., Jay Pantua, C. A., Zhou, B., Vital, B., Calautit, J., & Hughes, B. (2020). Numerical analysis of an urban road pavement solar collector (U-RPSC) for heat island mitigation: Impact on the urban environment. *Renewable Energy*.

Nwakaire, C. M., Onn, C. C., Yap, S. P., Yuen, C. W., & Onodagu, P. D. (2020). Urban Heat Island Studies with emphasis on urban pavements: A review. *Sustainable Cities and Society, 63*.

Rejeb, O., Dhaou, H., & Jemni, A. (2015). A numerical investigation of a photovoltaic thermal (PV/T) collector. *Renewable Energy, 77*, 43–50.

Rekioua, D., & Matagne, E. (2012). *Optimization of photovoltaic power systems: modelization, simulation and control*. Springer Science & Business Media.

Sakellariou, E., & Axaopoulos, P. (2018). An experimentally validated, transient model for sheet and tube PVT collector. *Solar Energy, 174*, 709–718.

Salari, A., Kazemian, A., Ma, T., Hakkaki-Fard, A., & Peng, J. (2020). Nanofluid based photovoltaic thermal systems integrated with phase change materials: Numerical simulation and thermodynamic analysis. *Energy Conversion and Management, 205*, Article 112384.

Swinbank, W. C. (1963). Long-wave radiation from clear skies. *Quarterly Journal of the Royal Meteorological Society, 89*(381), 339–348.

Tian, L., Lu, J., Li, Y., Bu, D., Liao, Y., & Wang, J. (2021). Temporal characteristics of urban heat island and its response to heat waves and energy consumption in the mountainous Chongqing. *China. Sustainable Cities and Society, 75*.

Tsoka, S., Theodosiou, T., Tsikaloudaki, K., & Flourentzou, F. (2018). Modeling the performance of cool pavements and the effect of their aging on outdoor surface and air temperatures. *Sustainable Cities and Society, 42*, 276–288.

Xiang, B., Yuan, Y., Ji, Y., Cao, X., & Zhou, J. (2020). Thermal and electrical performance of a novel photovoltaic-thermal road. *Solar Energy, 199*, 1–18.

Xie, P., & Wang, H. (2021). Potential benefit of photovoltaic pavement for mitigation of urban heat island effect. *Applied Thermal Engineering*, 191.

Yang, M., Zhang, X., Zhou, X., Liu, B., Wang, X., & Lin, X. (2021). Research and Exploration of Phase Change Materials on Solar Pavement and Asphalt Pavement: A review. *Journal of Energy Storage, 35*.

Yu, B., Liu, X., Li, N., Liu, S., & Ji, J. (2019). The performance analysis of a purified PV/T-Trombe wall based on thermal catalytic oxidation process in winter. *Energy Conversion and Management*, Article 112262.

Zaim, E. H., Farzan, H., & Ameri, M. (2020). Assessment of pipe configurations on heat dynamics and performance of pavement solar collectors: An experimental and numerical study. *Sustainable Energy Technologies and Assessments, 37*.

Zhao, W., Chen, X., Zhang, Y., Su, W., Xu, F., & Li, B. (2021). Deicing performances of a road unit driven by a hydronic heating system in severely cold regions of China. *Computers & Mathematics with Applications, 81*, 838–850.

Zhou, B., Pei, J., Hughes, B. R., Nasir, D. S. N. M., & Zhang, J. (2020). Analysis of mechanical properties for two different structures of photovoltaic pavement unit block. *Construction and Building Materials, 239*.

Zhu, X., Zhang, Q., Chen, L., & Du, Z. (2021). Mechanical response of hydronic asphalt pavement under temperature–vehicle coupled load: A finite element simulation and accelerated pavement testing study. *Construction and Building Materials, 272*.